Solar Energy Materials and Solar Cells 167 (2017) 133–139

Contents lists available at ScienceDirect

Solar Energy Materials and Solar Cells

journal homepage: www.elsevier.com/locate/solmat

Compensation of self-absorption losses in luminescent solar concentrators by increasing luminophore concentration

Zachar Krumer[a], Wilfried G.J.H.M. van Sark[b,*], Ruud E.I. Schropp[c], Celso de Mello Donegá[a]

[a] Condensed Matter and Interfaces, Debye Institute for NanoMaterials Science, Utrecht University, P.O. Box 80000, 3508TA Utrecht, The Netherlands
[b] Copernicus Institute, Utrecht University, Heidelberglaan 2, 3584 CS Utrecht, The Netherlands
[c] Eindhoven University of Technology, Department of Applied Physics, Plasma and Materials Processing, P.O. Box 513, 5600 MB Eindhoven, The Netherlands

ARTICLE INFO

Keywords:
Luminescent solar concentrators
Self-absorption
Lumogen Red
Lumogen Orange
Saturation
Solar cells

ABSTRACT

Self-absorption in luminophores is considered a major obstacle on the way towards efficient luminescent solar concentrators (LSCs). It is commonly expected that upon increasing luminophore concentration in an LSC the absorption of the luminophores increases as well and therefore self-absorption losses will have higher impact on the performance of the device. In this work we construct a fully functioning liquid phase LSC where the luminophore concentration can be altered without changing other conditions in the experimental set-up. We step-wise enlarge the concentration of the luminophores Lumogen Red 305 and Lumogen Orange 240, while monitoring the electrical output and self-absorption effects. Contrary to common belief, self-absorption does not increasingly limit the performance of LSCs when the luminophore concentration increases.

1. Introduction

Luminescent solar concentrators (LSCs) are photovoltaic devices whose goal is to reduce the necessary amount of active photovoltaic elements per Watt of delivered power by means of concentration [1]. The LSC device is essentially a thin transparent plate, within which luminescent species (luminophores) are dispersed (Fig. 1). Solar radiation enters the LSC through the large top surface and is absorbed by the luminophores. Subsequently the luminophores emit at a longer wavelength and into a different direction. A large fraction of the isotropically emitted light hits the inner surface of the transparent plate in the regime of total internal reflection and is therefore trapped inside the transparent plate. The trapped light is waveguided to the edges of the plate, where solar cells are attached and conversion into electricity takes place. Concentration arises from the projection of light entering through the large top surface onto the small solar cell surface, which makes it possible to harvest much more light per unit of semiconductor material. Unlike conventional geometric concentrators, this concentrator concept does not require bulky tracking devices and allows greater freedom when it comes to form, which makes it well suited for building integration of low-concentration photovoltaics [2–5].

Similarly to geometric concentrators, LSCs are not only characterized by their power conversion efficiency η_{LSC}, which is the ratio of the electric power output P_{LSC} and the incident radiative power Φ_{in}:

$$\eta_{LSC} = \frac{P_{LSC}}{\Phi_{in}} \tag{1}$$

which is a number that is smaller than the power conversion efficiencies of the solar cells involved. The actual concentration strength is given by the optical concentration factor C and compares the radiative power Φ_{LSC} incident on the solar cell attached to the edge of the LSC to the radiative power that is incident on the bare solar cell Φ_{SC}:

$$C = \frac{\Phi_{LSC}}{\Phi_{SC}} \tag{2}$$

Mainly the following loss mechanisms cause the performance of LCSs to be as yet rather low: non-radiative dissipation of the absorbed radiative energy by the luminescent species, the escape losses, i.e. the emission of light outside the waveguiding mode and the incomplete absorption of the incident light by the luminescence species. In addition to those there is also the issue of self-absorption. The emitted light can be re-absorbed by the luminescent species itself, which recycles photons including those that were already in waveguiding mode before self-absorption occurred. In this way photons are exposed to some of the loss mechanisms repeatedly and thus their effect is amplified.

A partial approach to solving the challenges has been offered by BASF with their Lumogen series [6,7]. The high luminescence quantum efficiency (95%), the ratio between the emitted and absorbed photons, of these perylene derivatives is one of the reasons that record LSC efficiencies were achieved with these dyes [8,9]. On the practical side

* Corresponding author.
E-mail address: w.g.j.h.m.vansark@uu.nl (W.G.J.H.M. van Sark).

http://dx.doi.org/10.1016/j.solmat.2017.04.010
Received 13 July 2016; Received in revised form 3 April 2017; Accepted 6 April 2017
Available online 13 April 2017

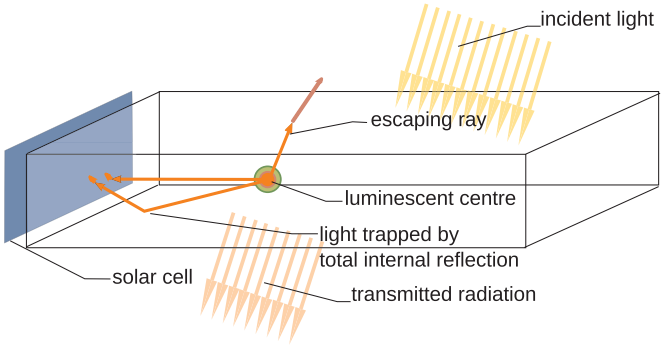

Fig. 1. Schematic representation of the working principle of a luminescent solar concentrator.

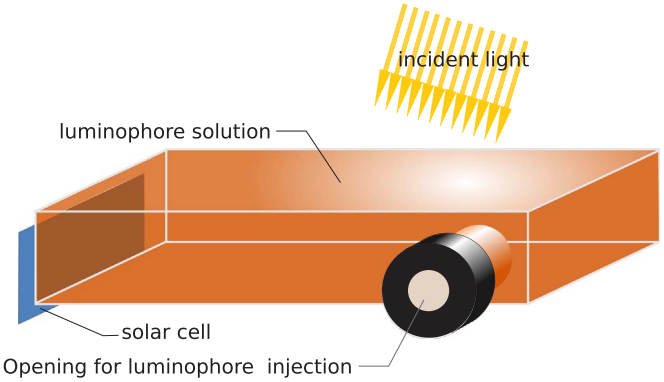

Fig. 2. Schematic representation of the liquid phase LSC system.

these dyes can be easily dispersed into PMMA [6] and passed long-term outdoor tests [10,11]. In fact Lumogen Red 305 is considered as the "working horse" of the LSC concept [12].

Organic dyes usually have narrow absorption bands when compared to semiconductor nanocrystals, which is why these have been receiving much attention in quantum dot LSCs [13,14]. In Lumogen Red 305 this can be overcome by enlarging the concentration of the dye, which increases absorption in the UV-region, as the law of Beer-Lambert predicts. This causes a gain in photon flux into the system and may lead in turn to a higher device output. However, the increase of overall absorption by enlargement of dye concentration simultaneously leads to an increase of self-absorption. These effects compete in reaching high device performance. In this work the concentration of Lumogen Red 305 is changed such that highest performance is reached, while monitoring the impact of self-absorption. Because of the competing effects we expect an optimal concentration for which the performance attains its maximum. We employ a *liquid* phase device, which allows the luminophore concentration to be easily and reliably changed, while keeping all other experimental parameters constant, such as coupling between the solar cell and the LSC, the quality of the transparent medium.

Because of the increase of the performance increasing effect (absorption) and the performance decreasing effects (self-absorption) with dye concentration an optimal concentration is expected at which the performance attains its maximum. The goal of this work is to critically evaluate the effects of luminophore concentration on the performance of LSCs.

2. Materials and methods

The monitoring of LSC performance and effects of self- absorption at various concentrations was carried out in two experiments: operation of a fully functional liquid phase prototype (Section 2.2) and spectroscopy at variable optical path lengths (Section 2.3). In both experiments the luminophore concentration was changed in a controlled way, such that data from both experiments was retrieved for the same range of luminophore concentrations. The scope of the work was widened by applying the procedure also to Lumogen Orange 240.

2.1. Luminophore solution

The commercially available BASF dyes Lumogen Red 305 (LR305) and Lumogen Orange 240 (LO240) were used to prepare a first highly concentrated stock-solution. The total mass of 120.8 mg LR305 was diluted in 10 ml toluene, while 7.8 mg LO240 was diluted in 10 ml acetone. Both solutions were used for the liquid phase prototype. The LR305 solution was diluted 12 times to obtain a second stock-solution for the spectroscopy at variable path lengths. The second solution was used to record the optical properties in standard cuvettes that are commonly used for absorption and luminescence spectroscopy (Section 2.3). The internal volume of these is 12 times smaller than the internal volume of the model LSC device, while the volume of the syringe used to add the stock solution to the measured solution was the same. Therefore the 12-fold dilution of the first stock solution for the second stock solution ensured that the luminophore concentrations were varied over the same range in both experiments. The absorption spectra of the individual concentrations were recorded using a Perkin-Elmer Lambda 950 spectrometer.

2.2. Model LSC device

The LSC was made from a custom-built quartz cuvette (Hellma Analytics) with the internal dimensions 100 mm × 35 mm × 10 mm. This cuvette is screw capped but the injection and removal of fluid is possible through the septum using a syringe (Fig. 2). Commercially available polycrystalline solar cells (14.56% (for Lumogen Red 305) and 15.13% (for Lumogen Orange 240) power conversion efficiency [15]) were used. Contacts were soldered to the back- and front side of the solar cell. For mechanical stability the cell was glued using a 3–5 mm thick layer of non-acidic silicone glue (Bison - transparent silicone sealant - Bi3311) on a glass substrate. The cell was covered with black absorber paper, which contained a window, such that the 35 mm × 10 mm facet of the cuvette could be placed in firm contact with the cell, while the remaining solar cell area was blocked from receiving light (Fig. 3). The cell was characterized by recording the current-voltage curves in the dark and under AM1.5 illumination, which yielded its efficiency. The efficiency measurements were carried out using class AAA [16] dual beam WACOM solar simulator [17]. It includes two light sources: a 1000-Watt Xenon lamp for the UV and visible part of the solar spectrum (below 700 nm) and a 300-Watt halogen lamp for the infrared part. The spectral mismatch is < 3% in the short wavelength ranges of interest here [18]. The current-voltage measurements were performed on a Keithley 238 High Current measure unit to characterize the bare solar cell, the LSC with pure solvent and the LSC with a luminophore solution at different concentrations. The cuvette was glued onto the solar cell using the adhesive MY-146, purchased from Mypolymers, which is refractive index matched to quartz (1.461 at 589 nm) [19]. The polymer was cured for a few seconds using a UV-lamp. Upon curing some air-bubbles appeared, which reduced the quality of optical coupling. The prototype with

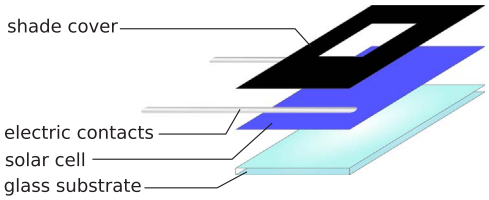

Fig. 3. Solar cell preparation for the liquid phase LSC device.

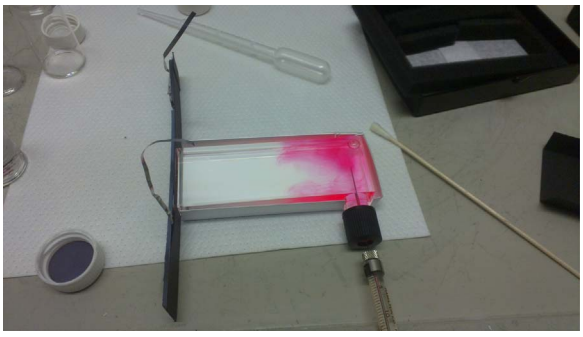

Fig. 4. A photograph of the model LSC being filled with Lumogen Red 305.

Lumogen Red 305 was coupled to the 14.56%-efficient poly-crystalline silicon solar cell while the prototype with Lumogen Orange 240 used the 15.13%-efficient solar cell. The optical coupling of the latter device was better due to a lower amount of amount of air-bubbles in the interface polymer layer.

The stock solution of luminophores was injected into the device through the septum using a Hamilton 25 µl syringe (Fig. 4) and subsequently the current-voltage characteristic of the device was measured. The luminophore concentration was increased in multiple controlled steps. After the injection of the luminophores the LSC was turned around multiple times to homogenize the solution. The quartz cuvette was wrapped into a multi- cellular polyethylene terephthalate-reflector (MCPET, Furukawa Electric [20]) such that all sides but the one facing the solar cell and the one facing the light source were covered. The LSC was placed on the measurement table of the solar simulator such that the gas bubble remained in the bottleneck and thus reflection from the air/luminophore solution interface did not contribute much to the light absorbed by the solar cell. The current-voltage characteristics were recorded while the LSC was illuminated for less than 5 s. For every measurement at least three measurements were taken. Since the illumination of the solar simulator is not perfectly homogeneous (< 2%, class AAA) and the quality of electrical contacts varied between measurements with a bias towards lower device output, the best value of all measurements for one concentration is presented here.

2.3. Spectroscopy at variable optical path lengths

To investigate the effect of self-absorption, emission spectra were measured in solution using an excitation source whose position and therefore the coordinate x (the distance from the aperture of optical fiber) of incidence on the luminescent material could be adjusted (Fig. 5). This way the distance between the entry spot of light and the detector can be varied in steps of 10 µm, such that the emitted light by luminescence travels along paths of different lengths through the luminescent solution. With increasing optical path, self-absorption effects become more and more prominent. In case of a strongly self-absorbing solution the luminescence signal weakens strongly as the distance x is increased, while a weakly self-absorbing sample would also weaken the luminescence signal albeit after a much longer distance x. The luminescent sample solutions were placed into a screw capped quartz cell with the internal volume of 10 mm × 10 mm × 35 mm. The bottom of the cell was brought in firm contact with an optical fiber, which was directed perpendicular to the direction of the excitation light and perpendicular to the x-axis along which the excitation light beam is moved. A range of optical paths between 5 mm and 30 mm was covered. The luminescence spectrum was recorded after each 0.5 mm step.

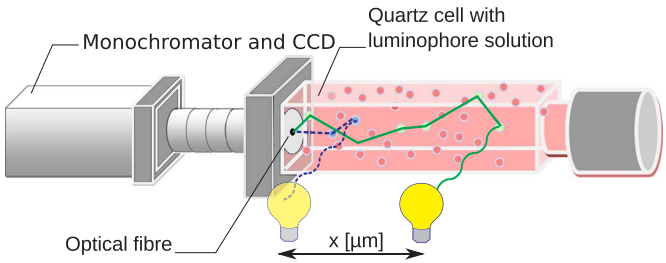

Fig. 5. Setup for spectroscopy at variable optical path lengths.

The measured spectra were integrated over wavelength to obtain the output intensity, which was normalized with respect to intensity at the shortest optical path (5 mm). These normalized intensity profiles were plotted against the corresponding x-coordinate.

For characterization the emission spectra were obtained from the intensity profile measurements of the intensity at the shortest optical path. A more detailed description is given in [14]. This procedure was repeated for luminophore solutions with the same dye concentrations as used for the model LSC device. The luminophore addition was carried out with a Hamilton 25 µl syringe through the septum in the screw cap of the cuvette.

3. Results and discussion

The efficiency of the LSC with increasing dye concentration is plotted in Fig. 6. The efficiency increases until saturation is reached. The saturation sets in at 57 ppm, which corresponds to the absorption spectra in Fig. 7. This saturation is expected from the Lambert-Beer law:

$$A = 1 - 10^{-\varepsilon c x} \tag{3}$$

which states that the fraction of absorbed light A increases and saturates as the dye concentration c at a constant absorption coefficient ε and a constant optical path x. In the actual LSC of 1 cm thickness, the optical path is at least twice as long because the light is reflected back from the reflector at the backside and it will have to pass the LSC at least one more time. Therefore the absorption properties of the LSC are described more accurately by the spectra for the optical path of 2 cm in Fig. 7 than for the conventional 1 cm. In this figure it is visible that at 57 ppm over a large spectral range more than 99% of light is absorbed.

The absorbed fraction of the incident AM1.5 spectrum α can be computed as a function of concentration of the luminophore c as follows:

$$\alpha(c) = \frac{1}{K_{AM1.5}} \int_0^\infty F_{AM1.5}(\lambda) A(c, \lambda) d\lambda$$
$$\text{with} K_{AM1.5} = \int_0^\infty F_{AM1.5}(\lambda) d\lambda \tag{4}$$

with $F_{AM1.5}(\lambda)$ being the incident AM1.5 spectrum, $A(c, \lambda)$ the absorption spectrum of the dye at the concentration c. This absorbed fraction is plotted against the concentration in Fig. 8. The plot with triangles in the

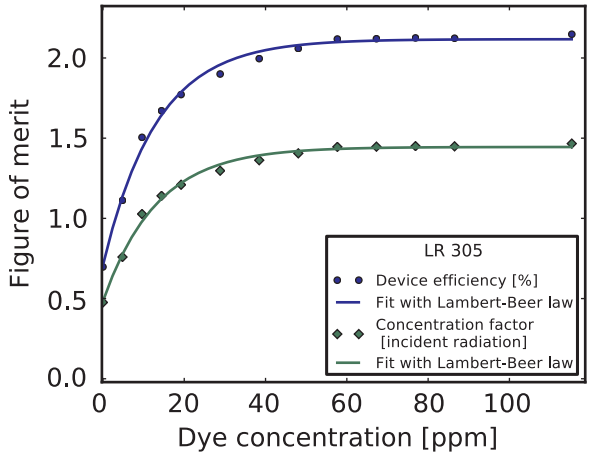

Fig. 6. Figures of merit: device efficiency and concentration factor as a function of increasing dye concentration of BASF Lumogen Red 305.

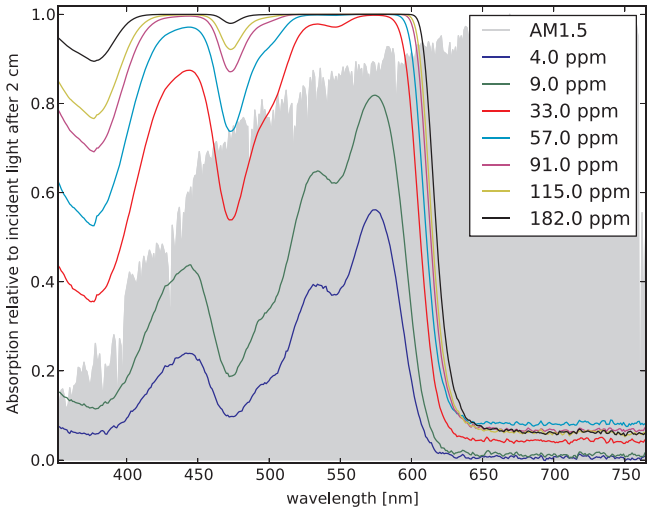

Fig. 7. Absorption Spectra of Lumogen Red 305 at different concentration after an optical path of 2 cm.

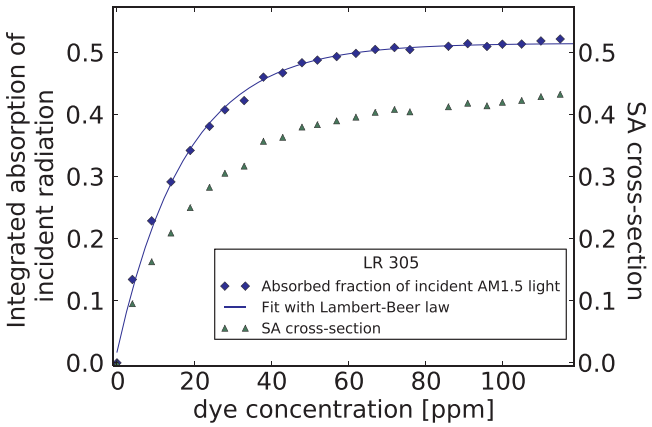

Fig. 8. Absorbed fraction of incident light from a AM1.5 light source as the concentration of LR305 increases.

Table 1
Fitting parameters for the graphs in Figs. 6 and 8 for the dependence of the figures of merit on the concentration c described by $A(1 - 10^{-Bc}) + C$ for Lumogen Red 305.

Parameter	Efficiency	Concentration factor	Absorption fraction
A	1.41	0.96	0.50
B	0.033	0.033	0.024
C	0.71	0.48	0.02

same figure represents the self-absorption cross-section, which is discussed in Section 3.1 below. The trends for the figures of merit (Fig. 6) and absorbed fraction are fitted to the Lambert-Beer law (Eq. (3), see also Table 1). The qualitative similarity indicates that increased absorption of incident light is a dominating effect upon increase of the dye concentration. We observed similar behavior with Lumogen Orange 240 (Fig. 9 and Table 2). However, using this dye the saturation of the device efficiency sets in at higher luminophore concentrations than the saturation of the light absorption. This is possibly caused by the different spectral position of the weaker near-UV absorption bands in the respective spectra: Lumogen Orange 240 has its weaker absorption band at 370 nm (see Fig. 10), where the AM1.5G intensity is very small, while Lumogen Red 305 has its weaker band at 450 nm, where the AM1.5G intensity is approximately three times higher. The increase of dye concentration contributes to the increase of the weaker absorption band in both solutions even after the primary absorption band is saturated. For Lumogen Orange 240 this increase contributes much

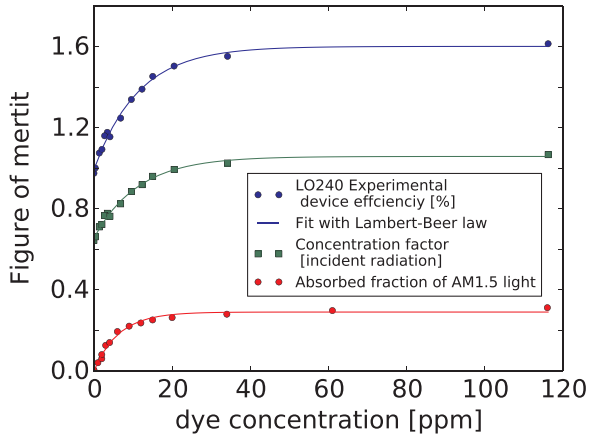

Fig. 9. Figures of merit: device efficiency, concentration factor and the fraction of absorbed light as a function of increasing dye concentration of BASF Lumogen Orange 240.

Table 2
Fitting parameters for the graphs in Fig. 9 for the dependence of the figures of merit on the concentration c described by $A(1 - 10^{-Bc}) + C$ for Lumogen Orange 240.

Parameter	Efficiency	Concentration factor	Absorption fraction
A	0.61	0.40	0.29
B	0.038	0.038	0.068
C	0.99	0.66	0.00

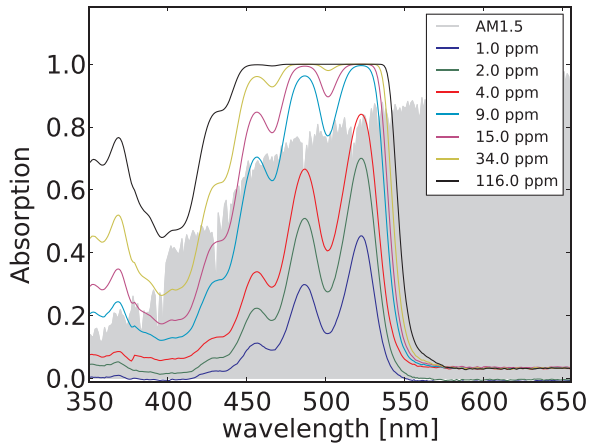

Fig. 10. Absorption spectra of Lumogen Orange 240 at different concentration after an optical path of 2 cm plotted over the AM1.5G incident spectrum.

fewer photons to the LSC than what is due to absorption by the main band. Thus saturation of the absorbed fraction sets in essentially with the saturation of primary absorption peaks. For the same reason increasing the concentration of Lumogen Red 305 still contributes to the increase of its absorption at 450 nm (see Fig. 7) even though the main peaks at 550–600 nm are already saturated. Thus increasing concentration still leads an increasing absorption fraction integrated over the spectral range of the whole AM1.5 spectrum.

3.1. Self-absorption

The contribution from the increasing photon flux that the system upon increasing luminophore concentration experiences, seems to compensate for the increasing self-absorption losses leading to a quasi concentration-independent overall device efficiency after the saturation is reached. This does not mean, however, that the self-absorption effects are weakened. On the contrary, self-absorption cross-section in- creases from 9.5% at 4 ppm to 43.3% at 115 ppm and to 50.0% at 336 ppm

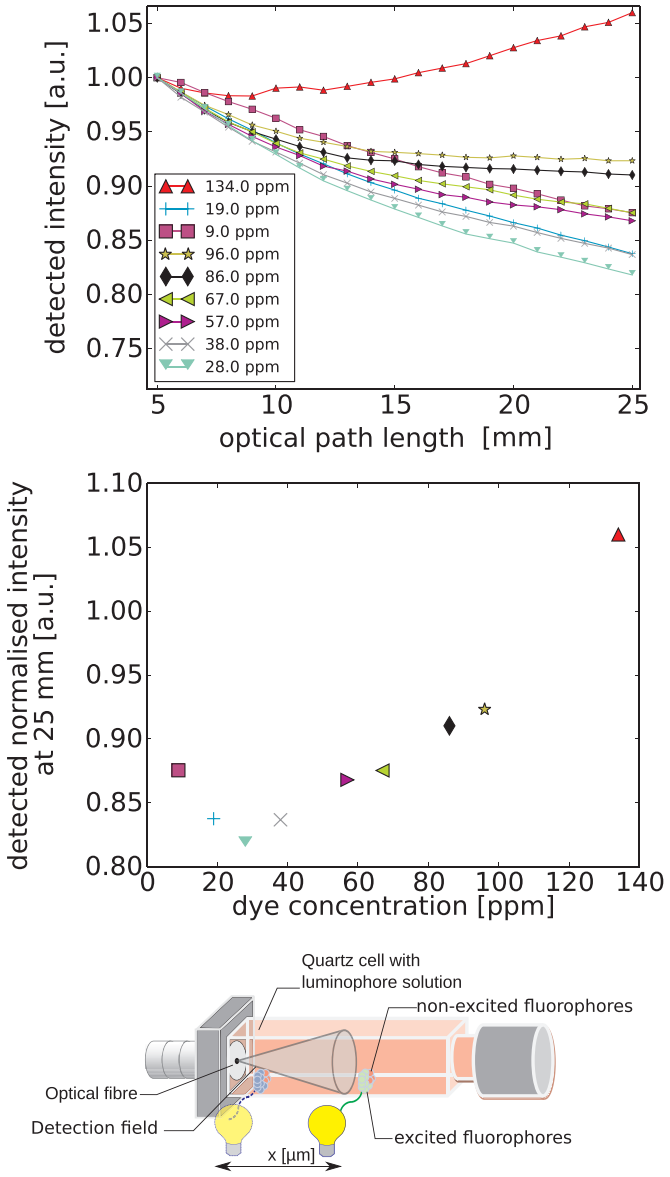

Fig. 11. Top: Normalized intensity profiles for Lumogen Red 305, Bottom: Effects observed in spectroscopy at variable optical paths at high concentration: The light emitted by the luminophores at longer optical paths is entirely emitted from an area whose light reaches the aperture of the optical fiber (from within the field of detection), while the light emitted at short optical paths is almost entirely outside the field of detection. Even though the luminescent light is attenuated more strongly at longer optical paths, at high concentration the detector in this set-up will receive a higher signal.

(Fig. 8). The self-absorption cross-section denotes the probability that the luminescence is absorbed by the luminophore itself after 2 cm of optical path length and is defined as:

$$\sigma(c) = \frac{1}{K_{LR305}} \int_0^\infty F_{LR305}(\lambda) A(c, \lambda) d\lambda$$
$$\text{with} K_{LR305} = \int_0^\infty F_{LR305}(\lambda) d\lambda \quad (5)$$

where $A(c, \lambda)$ is the absorption spectrum of the solution at the used concentration c after an optical path length of 2 cm and $F_{LR305}(\lambda)$ the emission spectrum of a sufficiently diluted solution of Lumogen Red 305, so that re-absorption can be neglected [14]. Direct evidence for self-absorption loss was collected by measuring the emission spectra at variable optical paths lengths and integrating the spectra to yield the total emission intensities. The results are shown in Fig. 11 (top). It can be clearly seen that the measured luminescence intensity decreases with

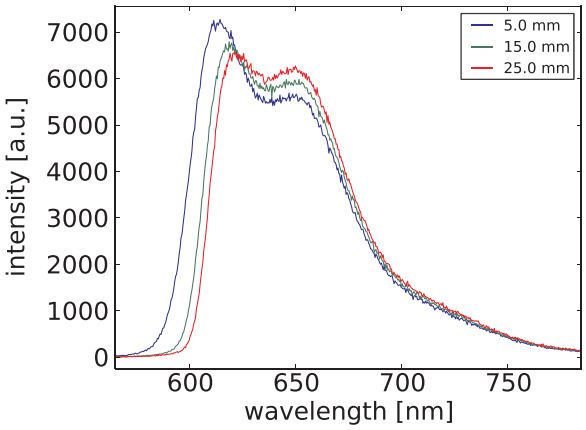

Fig. 12. Changes in emission spectra with increasing optical path for Lumogen Red 305 at a concentration of 96 ppm.

increasing optical path length.

This decrease in intensity is, however, not directly proportional to the increase of concentration as at higher dye concentrations most of the absorption and therefore luminescence takes place very close to the surface of the cuvette (i.e. the excitation light is absorbed within negligibly short optical paths after entering the cuvette, as expected from the exponential nature of the law of Lambert-Beer). Light from this region of maximum luminescence does not reach the detector at short optical paths as it is outside the conic detection field of the optical fiber. For longer optical paths the region of maximum intensity enters the detection field and the Fig. 11 (bottom). Thus it may occur happen that a higher signal is detected at sufficiently high concentrations and at long optical paths with high attenuation due to self-absorption compared to the signal for less attenuated luminescence at shorter optical paths. Such conditions have been reached for dye concentrations above 120 ppm. The recorded intensity spectra of the LSC edge emission reveal that the intensity decrease is mostly due to a de- crease in the blue part of the spectrum (Fig. 12). This decrease in the blue and a slight increase in the red are well detectable even at concentrations as high as 96 ppm, which is further evidence for the presence of self-absorption [14].

The experimental results suggest that the increase of dye concentration, even if it increases self-absorption losses, does not inhibit the device performance of LSCs, because the increase of absorbed radiation flux is large enough to compensate the self-absorption losses. This compensation can be described using the equation proposed by Olson et al. [21] in combination with the one proposed by Goetzberger and Greubel [1]:

$$\frac{\Phi_{LSC}}{\Phi_{in}} = \eta_{abs}(1 - \eta_{\text{int}})^{\langle N_{SA} \rangle} \quad (6)$$

where Φ_{LSC} is the radiation power flux of the LSC-edge emission, Φ_{in} the incident radiation power flux, η_{abs} the absorption efficiency of the luminophore solution, η_{int} the internal optical efficiency (the ratio of power of the LSC-edge emission and the absorbed incident power), and $\langle N_{SA} \rangle$ is the average number of self-absorption events per incident photon, which increases with η_{abs}. Both η_{abs} and $\langle N_{SA} \rangle$ increase with increasing dye concentration. The exponential nature of the photon recycling process due to self-absorption (described by the term $(1 - \eta_{\text{int}})^{\langle N_{SA} \rangle}$ dominates the device efficiency upon increase of concentration. That means that when η_{abs} is constant, the performance of the LSC drops. In case of Lumogen Red 305 within the range of dye concentration measured the absorption efficiency increases with concentration faster than $(1 - \eta_{\text{int}})^{\langle N_{SA} \rangle}$ decreases. This may be different for other luminophores with lower luminescence quantum efficiency and thus a resulting lower η_{int}. Similarly, larger self-absorption cross-section could contribute to a higher $\langle N_{SA} \rangle$.

Since the increased dye concentration did not reduce the device efficiency nor the optical concentration factor in spite of increased self-absorption, it is expected that the addition of near-UV absorbing dyes or other regions not yet covered by Lumogen Red 305 will increase the device efficiency also despite increasing self-absorption. That has been demonstrated by van Sark et al. by adding Fluorescence Yellow (CRS 040) to Lumogen Red 305 and increasing the efficiency from 2.4% to 2.7% [10]. At much higher dye concentrations the absorption in the near-UV comes close to 100% and thus the compensation of self-absorption losses stops. This is consistent with the findings of Kerrouche et al. who observed a drop in the radiative power of the edge emission of LSCs at dye concentrations above 1500 ppm [22].

3.2. Efficiency-optimized prototype

The data show that the device performance reaches saturation for dye concentrations above 60 ppm. Further increases in dye concentration result in minimal performance increase. We expect that at even higher dye concentrations the device efficiency will increase to a value only slightly larger than that measured so far. Thus to obtain a higher device efficiency we chose the best performing solar cell ($\eta_{SC}=15.13\%$) from our purchased batch to rebuild the liquid LSC and filled it with a Lumogen Red 305 solution with a concentration of 153 ppm. LR305 is preferred over LO240 as the performance of LO240 in our LSC experiments was already lower than that of Lumogen Red 305. Moreover the solubility of LO240 in acetone is smaller than the solubility of LR305 in toluene. For this rebuilt LSC a larger amount of index matching polymer was used to optically couple the solar cell to the quartz wall of the cuvette, yet again upon curing some air-bubbles appeared, though less than in the first LSC. Bubbles were pressed away along with the excess glue when the cuvette was pressed against the solar cell with the glue.

This way we are operating very close to the saturation efficiency. The measured device efficiency was 2.31% at an optical concentration factor of 1.53, with open-circuit voltage $V_{oc}=0.65$ V, short circuit current density $J_{sc}=0.53$ mA/cm^2, and fill factor $FF=0.67$. This is among the best-achieved efficiencies for LSCs with Lumogen Red and silicon cells. A comparison of LSCs reported in literature is given in Table 3 [4,23–26]. Although the LSC we fabricated does not set a new record in any single parameter it shows high values in all parameters. Judging from Table 3, clearly larger devices result in smaller device efficiencies, as in larger LSCs the optical path lengths are on average larger leading to larger self-absorption losses. In contrast to the case of increasing luminophore concentration, when the length and width of the LSC are increased the relative fraction of the light absorbed does not increase. Although in this way the aperture of the LSC becomes larger and more radiation is impinging on the LSC, this effect is cancelled out, as the incoming radiation calculated with respect to the aperture area in the device efficiency η_{LSC} is:

$$\eta_{LSC}=\frac{P_{LSC}}{P_{in}}=\frac{P_{LSC}}{L\cdot A_{top}} \tag{7}$$

where L is the power density of the light source (assumed constant over the area) and A_{top} is the aperture area of the LSC. Thus the enlarged aperture area decreases the device efficiency by the same factor by which it increases the absorbed light. Although we have shown this for relatively small dimension LSCs we expect that larger LSCs will be only slightly affected. This is corroborated by similar results obtained for long (> 1 m) LSC fibers [27], but also by outdoor test results for large area LSCs [28,29].

For an LSC in practice a high efficiency is not the only critical criterion. It is also important, that the concentrator delivers more power than the bare solar cell, otherwise it does not fulfill its purpose of concentration (i.e. $C<1$). This electrical concentration factor C^* is defined as the ratio of the electrical power delivered by the solar cell attached to the LSC-plate P_{LSC} and radiative power incident on the entire LSC aperture Φ_{in}. The latter can be calculated from the power density of the light source (assumed constant over the aperture area) L and the illuminated aperture area A_{top}. Thus the net effect of an increase of the dimensions of the LSC is an increase in optical path and thus an increase in parasitic absorption and self-absorption. The (optical) concentration factor C increases with LSC dimensions, because the geometrical concentration factor G does. The former is defined as the ratio of radiative power delivered to the solar cell attached to the LSC plate Φ_{LSC} and Φ_{SC} while illuminated under the same conditions:

$$C=\frac{\Phi_{LSC}}{\Phi_{SC}} \tag{8}$$

The geometrical concentration factor is given by the ratio of the collecting aperture surface A_{top} and the solar cell surface A_{SC}. If multiple solar cells are applied, then the total solar cell area is used, which is $n_{SC}a_{SC}$ for n_{SC} solar cells of identical size a_{SC}:

$$G=\frac{A_{top}}{A_{SC}}=\frac{A_{top}}{n_{SC}a_{SC}} \tag{9}$$

The two concentration factors can be combined using the optical efficiency of the LSC η_{opt}:

$$C=G\eta_{opt} \tag{10}$$

The radiative power delivered to the solar cell is converted into electrical power P_{LSC}. This occurs at efficiency η^*_{SC}, which is higher than the conventional solar cell efficiency η_{SC} under AM1.5 illumination, as the luminescent light of the LSC is emitted in a wavelength region of higher spectral response of the solar cell. The relationship between the electrical concentration factor C^* and the (optical) concentration factor C given by

$$C^*=\frac{L_{LSC}\eta^*_{SC}}{L_{SC}\eta_{SC}}=C\frac{\eta^*_{SC}}{\eta_{SC}}\geq C \tag{11}$$

Table 3
Highest reported LSC-efficiencies for Lumogen Red 305 and silicon cells according to [4]. The work of Hyldahl et al. [25] used only one solar cell attached to the LSC but projected their results for an LSC with four cells. The work of Gallagher et al. [24] has not been included, because the high efficiency of 3.3% reported there has been calculated with respect to the solar cell area and not to the area of the LSC surface exposed to illumination as in the listed works. The work of Corrado et al. [26] has been performed with a solar cell facing the illumination source and therefore could harvest the light not absorbed by the luminophores. #PV is the number of solar cells attached to the LSC in the experiment, G is the geometrical concentration factor, η_{SC} is the power conversion efficiency of the bare solar cell, η_{LSC} is the power conversion efficiency of the LSC with the attached solar cell and C^* is the electrical concentration factor of the device. The listed quantities are explained in the text.

Group	LSC size [cm]	#PV	G	η_{SC} [%]	η_{LSC} [%]	C^*	C^*/G [%]
Van Sark et al. [10]	5×5×0.4	1	12.5	18.6	2.4	1.61	12.9
Desmet et al. [23]	5×5×0.5	2	5	15.6	1.8	0.91	18.3
Desmet et al. [23]	10×10×0.5	2	10	15.6	1.8	1.20	12.0
Hyldahl et al. [25]	6.2×6.2×0.3	4	5.2	18.3	2.6	0.74	14.2
Corrado et al. [26]	31.8×31.8×0.476	12	3.4	19.8	6.8	1.2	35.6
Corrado et al. [26]	45.7×45.7×0.476	6	22.5	18.4	1.5	1.8	8
This work	3.5x10×1	1	10	15.13	2.3	1.53	15.3

In practice the concentration ratio of electrical power C^* is more relevant than the one of radiative power C. If compared using the criterion that the electrical concentration factor must be larger than one for a device to call it an effective concentrator, our device delivers the second best efficiency among LSCs with sideways oriented solar cells, surpassed only by the one of van Sark et al. [10], although it should be noted that C^* has not been calculated for many systems in older works. This is partially because the solar cell used in present work had a relatively poor efficiency of 15.13%. In the device we produced, the luminophores were dispersed in liquid toluene, which scatters light somewhat less than solid PMMA, which has been deployed in most other works as a matrix for the dye molecules. This reduced scattering allows us to achieve high efficiencies despite not using wavelength selective reflection layers as done by Goldschmidt et al. [9], van Sark et al. [10] and Desmet et al. [23].

4. Summary and conclusion

In this work we have demonstrated that despite present and increasing self-absorption in an LSC upon increasing Lumogen Red 305 dye concentration, the LSC device efficiency and the electrical concentration factor increase because of increasing absorption of incident light. An optimal dye concentration with respect to efficiency has not been found, however when considering material cost, especially the cost of dyes, a dye concentration at the saturation when device performance occurs will be most cost-effective. The investigation of optimum dye concentration with respect to costs is an interesting follow-up study.

We have fabricated an LSC with liquid dye solution with dye concentration as high as 153 ppm to present a working LSC device with one of the highest device efficiencies of all present concentrators using Lumogen Red 305.

The findings motivate a systematic follow-up study to investigate if the addition of a luminophore with high luminescence quantum efficiency and absorption in a different spectral region than the absorption of Lumogen Red 305 will result in significant increase of device efficiency.

Acknowledgements

This work is part of the Joint Solar Programme (JSP-2) of HyET Solar and the Stichting voor Fundamenteel Onderzoek der Materie FOM, which is part of the Netherlands Organisation for Scientific Research (NWO).

References

[1] A. Goetzberger, W. Greubel, Solar energy conversion with fluorescent collectors, Appl. Phys. 14 (1977) 123–139.
[2] D. Chemisana, Building integrated concentrating photovoltaics: a review, Renew. Sustain. Energy Rev. 15 (2011) 603–611.
[3] W.G.J.H.M. van Sark, Luminescent solar concentrators – a low cost photovoltaics alternative, Renew. Energy 49 (2013) 207–210.
[4] M.G. Debije, P.P.C. Verbunt, Thirty years of luminescent solar concentrator research: solar energy for the built environment, Adv. Energy Mater. 2 (2012) 12–35.
[5] B. Vishwanathan, A. Reinders, D. de Boer, L. Desmet, A. Rasa, F. Zahn, M. Debije, A comparison of performance of flat and bent photovoltaic luminescent solar concentrators, Sol. Energy 112 (2015) 120–127.
[6] G. Seybold, G. Wagenblast, New perylene and violanthrone dyestuffs for fluorescent collectors, Dyes Pigments 11 (1989) 303–317.
[7] A.F. Mansour, Optical efficiency and optical properties of luminescent solar concentrators, Polym. Test. 17 (1998) 333–343.
[8] L.H. Slooff, E.E. Bende, A.R. Burgers, T. Budel, M. Pravettoni, R.P. Kenny, E.D. Dunlop, A. Büchtemann, A luminescent solar concentrator with 7.1% power conversion efficiency, Phys. Status Solidi (RRL) - Rapid Res. Lett. 2 (2008) 257–259.
[9] J.C. Goldschmidt, M. Peters, A. Bösch, H. Helmers, F. Dimroth, S.W. Glunz, G. Willeke, Increasing the efficiency of fluorescent concentrator systems, Sol. Energy Mater. Sol. Cells 93 (2009) 176–182.
[10] W.G.J.H.M. van Sark, K.W. Barnham, L.H. Slooff, A.J. Chatten, A. Büchtemann, A. Meyer, S.J. Mc.Cormack, R. Koole, D.J. Farrell, R. Bose, E.E. Bende, A.R. Burgers, T. Budel, J. Quilitz, M. Kennedy, T. Meyer, C.D.M. Donegá, A. Meijerink, D. Vanmaekelbergh, Luminescent solar concentrators – a review of recent results, Opt. Express 16 (2008) 21773–21792.
[11] L.H. Slooff, N.J. Bakker, P.M. Sommeling, A. Büchtemann, A. Wedel, W.G.J.H.M. van Sark, Long-term optical stability of fluorescent solar concentrator plates, Phys. Status Solidi (a) 211 (2014) 1150–1154.
[12] M. Debije, P. Verbunt, P. Nadkarni, S. Velate, K. Bhaumik, S. Nedumbamana, B. Rowan, B. Richards, T. Hoeks, Promising fluorescent dye for solar energy conversion based on a perylene perinone, Appl. Opt. 50 (2011) 163–169.
[13] K. Barnham, J.L. Marques, J. Hassard, P. O'Brien, Quantum-dot concentrator and thermodynamic model for the global redshift, Appl. Phys. Lett. 76 (2000) 1197–1199.
[14] Z. Krumer, S.J. Pera, R.J. van Dijk-Moes, Y. Zhao, A.F. de Brouwer, E. Groeneveld, W.G.J.H.M. van Sark, R.E. Schropp, C. de Mello Donegá, Tackling self-absorption in luminescent solar concentrators with type-II colloidal quantum dots, Sol. Energy Mater. Sol. Cells 111 (2013) 57–65.
[15] Solar_rex, ⟨http://www.ebay.de/usr/solar_rex⟩.
[16] International Electrotechnical Commission, IEC 60904-3 Ed. 2.0, Photovoltaic devices – Part 3: Measurement principles for terrestrial photovoltaic (PV) solar devices with reference spectral irradiance data, 2008.
[17] Wacom Electric Co., ⟨http://www.wacom-ele.co.jp/en/products/solar/super/⟩.
[18] H. Li, Single and Multijunction Silicon Based Thin Film Solar Cells on a Flexible Substrate With Absorber Layers Made by Hot-Wire CVD (Ph.D. Thesis), Utrecht University, 2007.
[19] Mypolymers, ⟨http://www.mypolymers.com⟩.
[20] Furukawa Electric, ⟨https://furukawa.co.jp/mcpet/english/index.htm⟩.
[21] R. Olson, R.F. Loring, M. Fayer, Luminescent solar concentrators and the reabsorption problem, Appl. Opt. 20 (1981) 2934–2940.
[22] A. Kerrouche, D. Hardy, D. Ross, B. Richards, Luminescent solar concentrators: from experimental validation of 3D ray-tracing simulations to coloured stained-glass windows for {BIPV}, Sol. Energy Mater. Sol. Cells 122 (2014) 99–106.
[23] L. Desmet, A.J.M. Ras, D.K.G. de Boer, M.G. Debije, Monocrystalline silicon photovoltaic luminescent solar concentrator with 4.2% power conversion efficiency, Opt. Lett. 37 (2012) 3087–3089.
[24] S. Gallagher, B. Norton, P. Eames, Quantum dot solar concentrators: electrical conversion efficiencies and comparative concentrating factors of fabricated devices, Sol. Energy 81 (2007) 813–821.
[25] M.G. Hyldahl, S.T. Bailey, B.P. Wittmershaus, Photostability and performance of CdSe/ZnS quantum dots in luminescent solar concentrators, Sol. Energy 83 (4) (2009) 566–573.
[26] C. Corrado, S.W. Leow, M. Osborn, E. Chan, B. Balaban, S.A. Carter, Optimization of gain and energy conversion efficiency using front-facing photovoltaic cell luminescent solar concentrator design, Sol. Energy Mater. Sol. Cells 111 (2013) 74–81.
[27] O.Y. Edelenbosch, M. Fisher, L. Patrignani, W.G.J.H.M. van Sark, A.J. Chatten, Luminescent solar concentrators with fibre geometry, Opt. Express 21 (2013) A503–A514.
[28] N. Aste, L.C. Tagliabue, C. Del Pero, D. Testa, R. Fusco, Performance analysis of a large-area luminescent solar concentrator module, Renew. Energy 76 (2015) 330–337.
[29] L.H. Slooff, S. Verkuilen, M.M. de Jong, M.N. van den Donker, M. Kanellis, M.G. Debije, Luminescent solar noise barrier – large scale testing and modeling, in: Proceedings of the 32nd European Photovoltaic Solar Energy Conference and Exhibition, 2016, pp. 1375–1379.